Cellulose (2015) 22:1753–1762
DOI 10.1007/s10570-015-0615-1

ORIGINAL PAPER

Tailoring the yield and characteristics of wood cellulose nanocrystals (CNC) using concentrated acid hydrolysis

Liheng Chen · Qianqian Wang · Kolby Hirth · Carlos Baez · Umesh P. Agarwal · J. Y. Zhu

Received: 3 November 2014 / Accepted: 24 March 2015 / Published online: 1 April 2015

Abstract Cellulose nanocrystals (CNC) have recently received much attention in the global scientific community for their unique mechanical and optical properties. Here, we conducted the first detailed exploration of the basic properties of CNC, such as morphology, crystallinity, degree of sulfation and yield, as a function of production condition variables. The rapid cellulose depolymerization and sulfation reactions under concentrated acid concentrations of around 60 wt% resulted in a very narrow operating window for CNC production. We found that CNC yields as high as 70 wt% from a bleached eucalyptus kraft pulp with glucan content of 78 wt% can be achieved under a tight range of reaction conditions and that a weighted average length of over 200 nm and sulfur content (a measure of CNC surface charge) between 3 and 10 mg/g can be produced. This study provided critical knowledge for the production of CNC with characteristics tailored for different specific applications, significant to commercialization.

Keywords Cellulose nanocrystals (CNC) · Crystallinity · Crystal length and morphology · Surface charge · CNC yield optimization · Concentrated acid hydrolysis

Introduction

Cellulose nanocrystals (CNC), as a renewable nanomaterial, can be sustainably produced in large quantities using the abundant natural lignocelluloses available in many geographic regions on earth. CNC recently received great attention in the global scientific community for their unique mechanical and optical properties (Dong and Gray 1997; Habibi et al. 2010; Revol et al. 1994; Šturcová et al. 2005). Potential

This work was conducted on official government time of Zhu, Hirth, Baez, and Agarwal and while Chen and Wang were visiting students at the USDA Forest Products Lab.

Electronic supplementary material The online version of this article (doi:10.1007/s10570-015-0615-1) contains supplementary material, which is available to authorized users.

L. Chen
State Key Lab of Pulp Paper Engineering, South China University Technology, Guangzhou, China

L. Chen · Q. Wang · K. Hirth · C. Baez · U. P. Agarwal · J. Y. Zhu (✉)
Forest Products Laboratory, USDA Forest Service, Madison, WI, USA
e-mail: jzhu@fs.fed.us

Q. Wang
Biofuels Institute, School of the Environment, Jiangsu University, Zhenjiang, China

J. Y. Zhu
Department of Biological Systems Engineering, University of Wisconsin, Madison, WI, USA

applications include lightweight and mechanically adaptive nanocomposites (Capadona et al. 2008; Hsu et al. 2011; Xu et al. 2014), solar cells (Zhou et al. 2013), photonics (Kelly et al. 2013), light-healable supramolecular composites (Biyani et al. 2013; Coulibaly et al. 2014), drug delivery (Potter et al. 2014), and LED display and smart windows by substituting non-renewable liquid crystals. All these promising applications strongly depend on the inherent chemical, physical, and optical properties of CNC, as well as the ability for subsequent chemical modification. Therefore, having a controlled production process to obtain desired CNC properties is of vital importance.

CNC are commonly produced by acid hydrolysis of cellulosic fibers, and the literature reflects much work in this area. Sulfuric, phosphoric, and hydrochloric acids have been used (Camarero Espinosa et al. 2013; Dong et al. 1998; Mukherjee and Woods 1953; Yu et al. 2013). Using sulfuric acid, the reduction of cellulose degree of polymerization (DP), sulfation of cellulose, and production of CNC occurs abruptly and simultaneously (Hamad and Hu 2010; Wang et al. 2012). As a result, process control and optimization are very difficult. For decades, the standard condition has been approximately 64 wt% sulfuric acid for producing CNC with good dispersion properties, due to the formation of sulfate groups that impart electrostatic stability, important for aqueous processing (Araki et al. 1998; Beck-Candanedo et al. 2005; Chen et al. 2009; Marchessault et al. 1961; Mukherjee and Woods 1953; Revol et al. 1994). A sulfuric acid concentration of 60 wt% (<64 wt%) was used for producing CNC film (Revol et al. 1997); however, the study did not report CNC yield or morphological properties.

Low CNC yields (of approximately 30 wt%) have been the main drawback using sulfuric acid concentrations reported in the literature. Traditional statistical experimental designs for optimizing CNC production (Bondeson et al. 2006; Hamad and Hu 2010) resulted in low CNC yields of approximately 35 % because they were unable to resolve the abrupt change in CNC yield at acid concentrations between 56 and 58 wt%. Recently we demonstrated that only a slightly lower sulfuric acid concentration (58 wt%) resulted in near zero loss of cellulose to sugars, and created the possibility to substantially improve CNC yield (Wang et al. 2012). We later conducted a kinetic study (Wang et al. 2014) which verified the abrupt CNC production phenomenon at acid concentration between 56 and 58 wt%, and demonstrated that acid concentration is the key parameter to control CNC production. Below 58 wt% only a very small amount of CNC are produced due to insufficient cellulose depolymerization, while above 62 wt% the CNC are rapidly hydrolyzed to glucose, also resulting in low yield. This finding provides a mechanism for controlling CNC yield by simply controlling acid concentration. Laboratory bench scale experiments verified that CNC yield of over 70 wt% was achievable using a bleached eucalyptus pulp with xylan content of approximately 15 % (Wang et al. 2014), which substantially improves the economics of CNC production for commercial applications.

The immediate question to be asked, then, is whether or not acid concentration can be used to control desired CNC properties. The properties of the wood CNC were found to be not much affected by varying other hydrolytic conditions such as temperature and reaction time at the standard acid concentration of 64 wt% (Beck-Candanedo et al. 2005). Kenaf bast fiber CNC from 65 wt% sulfuric acid at 45 °C were reported to have decreased width (from 13 to 11 nm), but no change in length, as hydrolysis time increased (Kargarzadeh et al. 2012). Microcrystalline cellulose CNC were reported to have varied crystal length under other hydrolytic conditions using 6 N HCl (Yu et al. 2013) and have been reported to aggregate (Araki et al. 1998). Here we demonstrate that CNC properties, such as crystal length, crystallinity, and surface charge are directly related to acid concentration in sulfuric acid hydrolysis of a bleached eucalyptus kraft pulp. The importance of this study is that the production of CNC can be tailored to a specific application. For example, CNC with large aspect ratio (or long crystal length) may be most desirable for polymer reinforcement in cellulose nanocomposite production, while low aspect ratio CNC with uniform crystal length and high crystallinity may be more suitable for smart windows or LED displays to replace non-renewable liquid crystals.

Materials and methods

Materials

A bleached eucalyptus kraft dry lap pulp (BEP) was obtained from a commercial source (Aracruz Cellulose, Brazil). The dry lap was disintegrated into a fiber

suspension at 5 % solids using a commercial disintegrator (Model 73-06-01, TMI, Ronkonkoma, New York, USA) at 312 rpm for 5000 revolutions after soaking in water overnight. The wet pulp was then vacuum dewatered and air dried to approximately 8 % moisture. The chemical composition of the fibers was 78.1 wt% glucan, 15.5 wt% xylan, and 0.1 wt% lignin, analyzed using a two-step acid hydrolysis procedure (Luo et al. 2010) together with a high-performance anion exchange chromatographic method using pulsed amperometric detection (HPAEC/PAD) (Davis 1998). The air dried fibers were used to produce CNC by concentrated acid hydrolysis. Sulfuric acid ACS reagent grade was purchased from Sigma-Aldrich (St. Louis, MO).

CNC production

The same procedure described in our previous studies was employed to produce CNC (Wang et al. 2014, 2012). Sulfuric acid concentration and reaction temperature were varied in ranges between 50–64 wt% and 35–80 °C, respectively. Reaction time was varied in a range of 15–240 min. We use (A in wt%, T in °C, t in min) to abbreviate hydrolysis conditions in the following discussion. All acid hydrolysis experiments were conducted using a 1:10 (g/mL) ratio of fiber solids (in oven dry weight) to acid solution. The reaction stream was sampled periodically using a pipet to obtain time-dependent information of the reactants and products, including CNC yield and properties. Each sampled material was immediately diluted to eightfold by volume with de-ionized (DI) water to quench the hydrolysis reaction. The precipitate was separated after centrifugation at 9000 rpm and then dialyzed using DI water until constant pH was reached. The resulting suspension was centrifuged again at 9000 rpm to separate the CNC.

CNC yield

Chemical oxygen demand (COD) measurements were used to determine both CNC yield and the remaining partially hydrolyzed, precipitable cellulose solid residue (CSR). The colorimetric COD measurements were conducted in commercial Accu-test^{TM} COD test vials (Biosciences, Inc., Bethlehem, PA, USA, ISO 9001:2000 certified). The amount of organics consumed, corresponding to the measured COD, was assumed to be all cellulose and can be calculated as $m_{\text{Cellulose}}$ (mg/L) = 2877.6 × I^{600} through calibration using avicel. This COD method was verified with a gravimetric method previously described (Wang et al. 2012).

TEM and morphology

Transmission electron microscopy (TEM) was used to examine the CNC morphology and determine crystal length. CNC suspensions of 0.1 g/L were diluted and sonicated to disperse the crystals. TEM grids (ultrathin carbon films supported by fenestrated carbon films) were floated on drops of approximately 5 μL sample for 1–2 min. They were then swished through two consecutive 250 μL drops of 2 % aqueous uranyl acetate. Excess stain was removed by capillary action and gentle blotting resulting in negatively stained particles. The samples were imaged using a Philips CM100 transmission electron microscope (FEI Company, Portland OR) with an accelerating potential of 100 keV. Images were captured on an SIA L3C 4-2 Mpixel CCD camera (Scientific Instruments and Application, Duluth, GA, USA). The magnification bars on the images were calibrated using replica grating or asbestos lattice. The number of crystals in TEM images for each sample counted ranged from 50 to 350 crystals. The low number of 50 was due to the low CNC yield for samples produced at low acid concentrations (≤56 wt%). Individual crystal length was determined by Image J 1.47 v (National Institute of Health, USA). Sufficient sample dilution was used to reduce potential CNC agglomeration in TEM imaging to facilitate CNC crystal length measurements.

Crystallinity

Wide-angle X-ray diffraction measurements of CNC samples were made using a Bruker D8 Discover system with Cu–Kα radiation (Bruker Corp., Billerica, MA) at the Material Science Center, University of Wisconsin, Madison, WI. The instrument features a 2D detector with a 14 cm diameter active area and a resolution of 2048 × 2048 pixels. A spot size of 0.5 mm was used. Scattering signals were collected in a 2 min period for every specimen. The CNC suspensions were first freeze-dried to avoid film formation and to minimize the potential for preferred orientation in the samples. The freeze-dried CNC samples were

pressed into 100 mg, 8 mm diameter pellets using hydraulic compression (180 MPa), according to the Segal method (Segal et al. 1959). To calculate the crystallinity index (*CrI*), the intensity of the (200) diffraction and the amorphous contribution (at $2\theta = 18°$) were measured. The *CrI* was then determined according to the Segal method: $CrI = 100 \times (I_{200}-I_{200})/I_{200}$ with I_{am} the intensity at $2\theta = 18°$. The average of duplicate measurements was reported and standard deviations were used as error bars in plotting.

To verify the *CrI* measurements using the Segal method, the X-ray diffraction data for selected samples were also fitted using the Rietveld–Ruland model (Fig. S1). The samples were also analyzed using Raman spectroscopy to determine *CrI* (Table S1) based on the ratio of the Raman scattering intensities at 380 and 1096 cm^{-1} (Agarwal et al. 2010).

Sulfur content

The sulfur content of each CNC and CSR sample was analyzed using an ICP–AES (Ultima II, Horiba Jobin–Yvon, Edison, NJ, USA) to represent the cellulose surface sulfation or charge. An aliquot of 5 or 10 mL CNC or CSR suspension was transferred to a Teflon digestion flask and digested at 150 °C for 30 min in a microwave (MDS-2000, CEM Corp., Matthews, North Carolina, USA) with approximately 5 mL of 70 % HNO_3 before ICP–AES analysis. The ramp time for digestion at 150 °C was approximately 40 min. All samples were run sampled and analyzed in duplicate. Two sets of CNC samples from 62 wt% acid, (62, 50, t) and (62, 60, t), were later repeated in triplicate to verify results. The average values from all replicate analyses were used for data presentation and the standard deviations were used as error bars in plotting. Because aqueous solutions were directly sampled and analyzed, it is believed that the measured sulfur content includes sulfate ions in the electrical double layer (Beck et al. 2011).

Results and discussion

Maximal CNC yield

A maximal CNC yield at a given acid concentration was determined experimentally by varying reaction temperature and time, where acid concentrations were varied between 50 and 64 wt%. Plotting maximal CNC yields as a function of sulfuric acid concentration reveals that acid concentration of 58 wt% is a transition point (Fig. 1) below which only a small amount of CNC, approximately <30 %, were produced in the temperature range studied. This can be attributed to insufficient deploymerization of cellulose (Hamad and Hu 2010). Most of the remaining fibers were in the form of partially hydrolyzed CSR. High CNC yield was achieved only with acid concentration of 58 wt% or higher and, accordingly, CSR yield rapidly decreased as acid concentration was increased over 58 wt%. This sharp transition point, at acid concentration 58 wt%, in CNC yield illustrates the difficulties in optimizing CNC yield using traditional statistical experimental design, as reported in previous studies with large acid increment step and over wide acid ranges (Bondeson et al. 2006; Hamad and Hu 2010) and led to the common belief that CNC can only be produced in significant yield by using acid concentration of approximately 64 wt%.

The three maximal CNC yields at 56 wt% acid, achieved at different hydrolysis temperatures 50, 60, and 70 °C by varying reaction time, were also plotted in Fig. 1 to illustrate that increasing temperature does not significantly improve yield at low acid concentrations. Overall, acid concentration is the governing parameter controlling CNC and CSR yields, except at

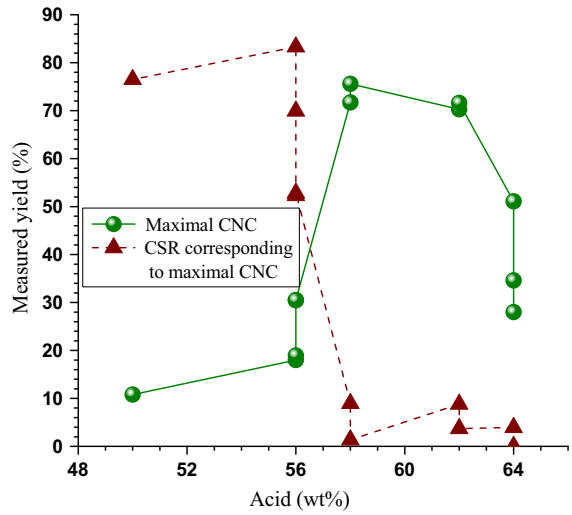

Fig. 1 Effect of sulfuric acid concentration on measured maximal yield of cellulose nanocrystal (CNC) in the range of temperature and reaction time studied and the corresponding yield of cellulosic solid residue (CSR)

high acid and long hydrolysis times where cellulose dissolution becomes dominant.

CNC morphology

Acid concentration also affected the morphology of the resultant CNC as revealed by TEM imaging (Figs. 2a–i). Comparisons of typical TEM of CNC samples corresponding to the data points in Fig. 1 indicate that overall crystal length decreased with increasing acid concentration. To quantitatively illustrate this, the length weighted average crystal length, $L_{21} = \frac{\sum_1^N n_i L^2}{\sum_1^N n_i L}$, was calculated and compared as shown in Fig. 3a, despite sample sizes of 30–350 crystals being statistically suboptimal. The maximal CNC L_{21} at a given acid concentration, which also approximately corresponds to the maximal CNC yield, decreased linearly with acid. The maximal L_{21} was approximately 280 nm at acid concentration 56 wt%, almost two times that of that at concentration of 64 wt%. L_{21} also decreased with increasing hydrolysis time for acid concentrations of 58 and 64 wt% (Fig. 3b).

The above discussion suggests that the reduction of CNC length is dictated by the extent or severity of hydrolysis reaction. To further illustrate this, we compared the crystal length distribution for three runs at different reaction conditions. L_{21} was 130.5 nm for run at (64, 45, 105) compared with $L_{21} = 189.3$ nm for (62, 60, 30), and $L_{21} = 228.2$ nm for (58, 56, 180). Furthermore, the distribution was narrower for (64, 45, 105) than that for (62, 60, 30) and for (58, 56, 180). Notice the x coordinate in Fig. 3c is logarithmic scale. The crystal length distribution for (56, 70, 90) was similar to that for (58, 56, 180) with a slight shift to the longer length (not shown in Fig. 3c for clarity).

At low acid concentration of 56 wt%, insufficient depolymerization of cellulose was also evident in TEM images (Fig. 2a) of nanofibril-like particles, rather than CNC-like morphology. Under moderate acid concentrations of 58 and 62 wt%, CNC morphology varied little among runs with similar yield and at the same acid concentration with different temperatures and appropriate reaction times (Compare Figs. 2b with c, 2e with f, g). At acid concentration of 64 wt% and reaction temperature of 45 °C, CNC from short reaction times had dramatically different visual appearance from those at long reaction time ($\geq$75 min) as can be seen from Figs. 2h and i. This difference most likely was caused by the difference in staining for TEM imaging. The negative staining can be affected by sample surface properties, such as morphology, e.g. the crisscross structure in Fig. 2h, curvature, charge, hydrophobicity. The small amount of xylan and some non-crystalline cellulose remained in the sample (Fig. 2h) (Wang et al. 2014) that are more hydrophilic than crystalline cellulose also affect staining. Therefore, the difference in TEM imaging appearance reflected the difference in CNC morphological and chemical properties. The CNC yield data (Fig. 1) suggest that more cellulose (most likely disordered) was degraded into glucose at longer reaction times, as validated by glucose measurements (Wang et al. 2014) resulting in CNC with higher crystallinity, as will be discussed in the following section.

CNC crystallinity

The original bleach eucalyptus pulp fibers (BEP) have an average *CrI* of 76.0 $\pm$ 0.4 % based on 4 replicate measurements. The change in CNC *CrI* was a result of hydrolysis and should be correlated to the extent of hydrolysis or reaction severity. This is supported by the general trend of *CrI* increased with acid concentration (Fig. 4a) because acid was the dominant factor in the hydrolysis reactions as discussed previously. Increasing reaction time also increased *CrI* especially at high acid concentrations (Fig. 4b). Reaction time had negligible effect at acid concentration of 58 wt%. The X-ray scattering intensity patterns of selected CNC samples are shown in Fig. 4c along with that of the BEP fibers for comparison purpose. The disappearance of the signal at $2\theta \approx 18°$ corresponding to amorphous materials was obvious as acid concentration was increased.

For acid concentrations above 58 %, CNC yield should be inversely correlated to *CrI* because of the accessibility and preferential hydrolysis of the more disordered regions. As expected, the CNC sample with lowest yield was the most crystalline (Fig. 4d). Here we are only interested in discussing CNC produced from acid concentrations $\geq$58 wt% because of the low amounts of CNC produced below 58 wt%. At moderate to low hydrolysis severities, such as at acid concentration of 58 %, the slope was close to zero

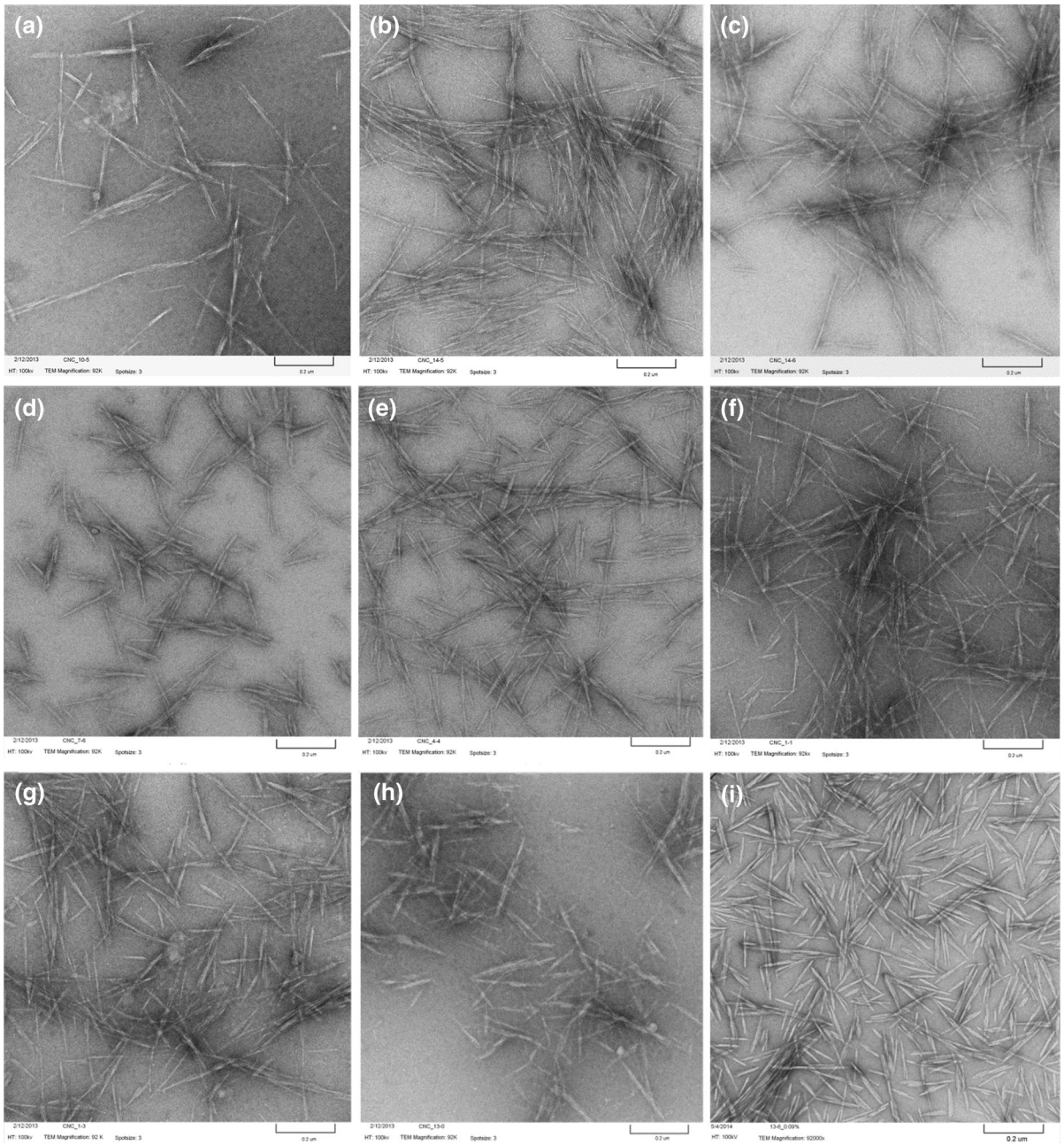

Fig. 2 TEM images of cellulose nanocrystals (CNC) produced at different reaction conditions. All scales = 200 nm; Y = CNC yield. **a** (56, 70, 90), Y = 30.0 %, L_{21} = 281.2 nm; **b** (58, 56, 180), Y = 71.7 %, L_{21} = 228.2 nm; **c** (58, 56, 210), Y = 75.6 %, L_{21} = 204.6 nm; **d** (62, 40, 105), Y = 64.8 %, L_{21} = 177.1 nm; **e** (62, 50, 75), Y = 70.3 %, L_{21} = 143.0 nm; **f** (62, 60, 30), Y = 71.6 %, L_{21} = 189.3 nm; **g** (62, 60, 60), Y = 69.4 %, L_{21} = 149.0 nm; **h** (64, 45, 15), Y = 51.1 %, L_{21} = 147.6 nm; **i** (64, 45, 105), Y = 28.0 %, L_{21} = 130.5 nm

because CNC yield was no longer solely dictated by CNC degradation but also dependent upon sufficient depolymerization of cellulose. *CrI* was only approximately 73 % for CNC samples produced at acid concentration 58 wt% (shown in Figs. 2b, c) while yield was as high as 75 %. In other words, less than even 10 % of the original cellulose was degraded to sugars (the measured glucan content of the BEP fibers

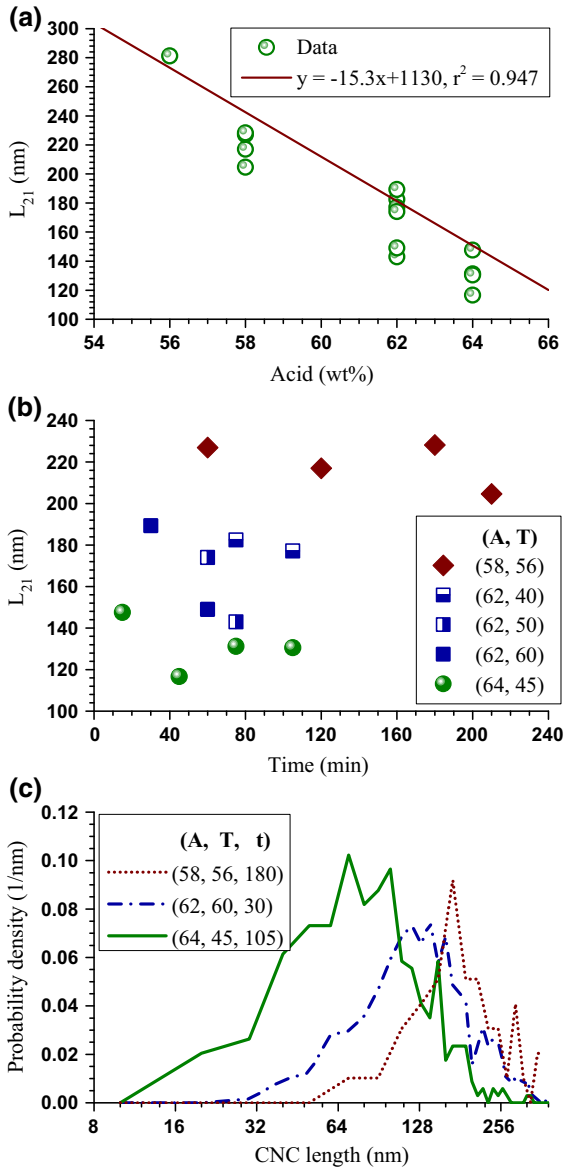

Fig. 3 CNC crystal length weighted average length L_{21} along with length probability distribution under different reaction conditions. **a** Acid concentration effect; **b** Reaction time effect; **c** CNC length distribution probability density function for three CNC samples from different reaction conditions

was 78 %), which resulted in minimal change in the *CrI* of the resultant CNC. By contrast, the *CrI* decreased with CNC yield linearly at higher acid concentrations of 62 and 64 wt%. It is noticed few CNC samples had *CrI* higher than the *CrI* of original BEP. The accuracy of the absolute *CrI* measurements is still an issued to be studied (Park et al. 2010).

CNC sulfation

CNC sulfur content was used to measure the degree of sulfation or surface charge. Acid concentration was a dominant factor affecting sulfation, but is also influenced by reaction temperature and time (Fig. 5a). Maximal sulfur content increased with acid concentration up to 62 wt% and then decreased with further increase in acid concentration. The sulfur content of CSR is lower than CNC, in general (Fig. 5a). The extent of sulfation was directly associated with the degree of hydrolysis reactions. CSR resulted from insufficient hydrolysis of initial fibers and therefore had lower sulfur content than CNC. It was recognized that concentrated acid hydrolysis is responsible for the electrical double layer due to trapped sulfate ions in the bound-water layer (Beck et al. 2011). The double layer phenomenon may be more pronounced at higher acid concentrations resulting in higher sulfur content (Figs. 5b, d).

The results also illustrate that CNC sulfation occurred rapidly except at low acid and temperature (56 wt%, 50 °C or below,)—and then slowed substantially (Fig. 5b). Interestingly, the 64 wt% acid run showed desulfation beginning in <1 h, which we attribute to the degradation of sulfated CNC to sugars (Fig. 1); the desulfation tapers off after about 2 h. The highest sulfur content was obtained at acid concentration of 62 wt% and 60 °C for approximately 100 min. Slight reductions with time were observed at (62,50, t) and (62, 60, t).

Cellulose sulfation and depolymerization are indicative reactions of CNC formation (Hamad and Hu 2010; Wang et al. 2012). CNC sulfur content was plotted against CNC yield (Fig. 5c). CNC degradation to sugar was low at acid concentration below 64 wt% (Fig. 1), therefore the measured CNC sulfur content was proportional to yield and suggests that more CNC were formed as cellulose was being sulfated. At 62 wt% acid and ≥50 °C, the sulfation reaction was rapid and resulted in very high CNC yield of approximately 70 % within the first 30 min and with very low subsequent CNC degradation (Wang et al. 2014). The plot of sulfur content versus yield is almost a vertical line for all measured reaction times (Fig. 5c). At 64 wt% acid, degradation became important after 15 min hydrolysis, which also resulted in reduced sulfur content as well as CNC yield, i.e., proportional relationship

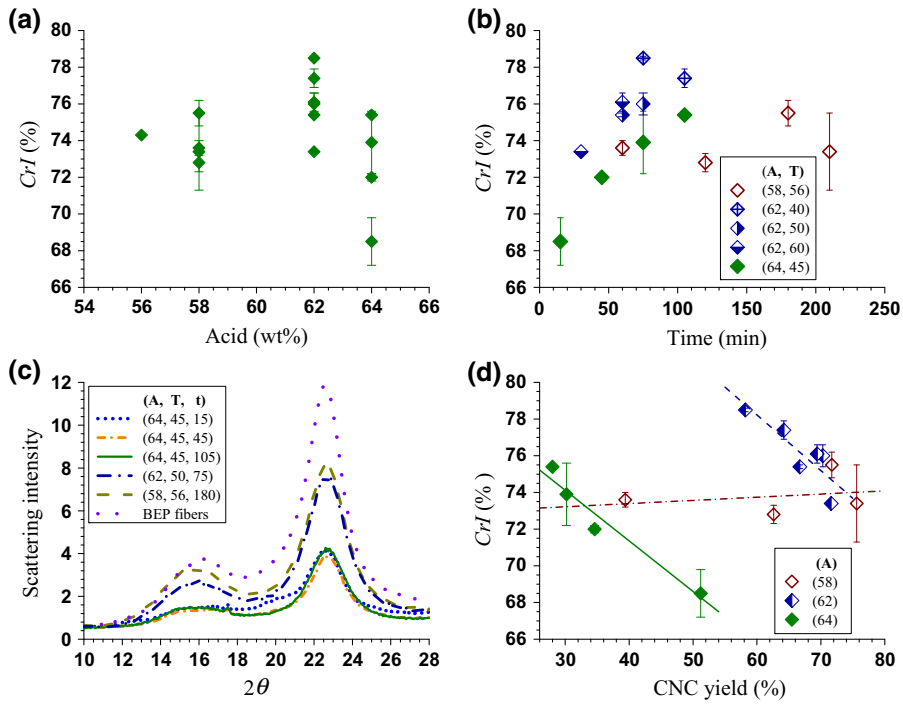

Fig. 4 CNC crystallinity (*CrI*). **a** Effect of acid concentration on *CrI*; **b** Effect of reaction time on *CrI*; **c** Angular intensity distribution of X-ray diffraction by different CNC samples; **d** correlations between *CrI* and CNC yield at different acid concentrations, *dashed line with dot* $y = 72.7 - 0.002x$, $r^2 = 0.39$, *dashed line* $y = 96.4 - 0.30x$, $r^2 = 0.68$, *solid line* $y = 82.4 - 0.28x$, $r^2 = 0.92$

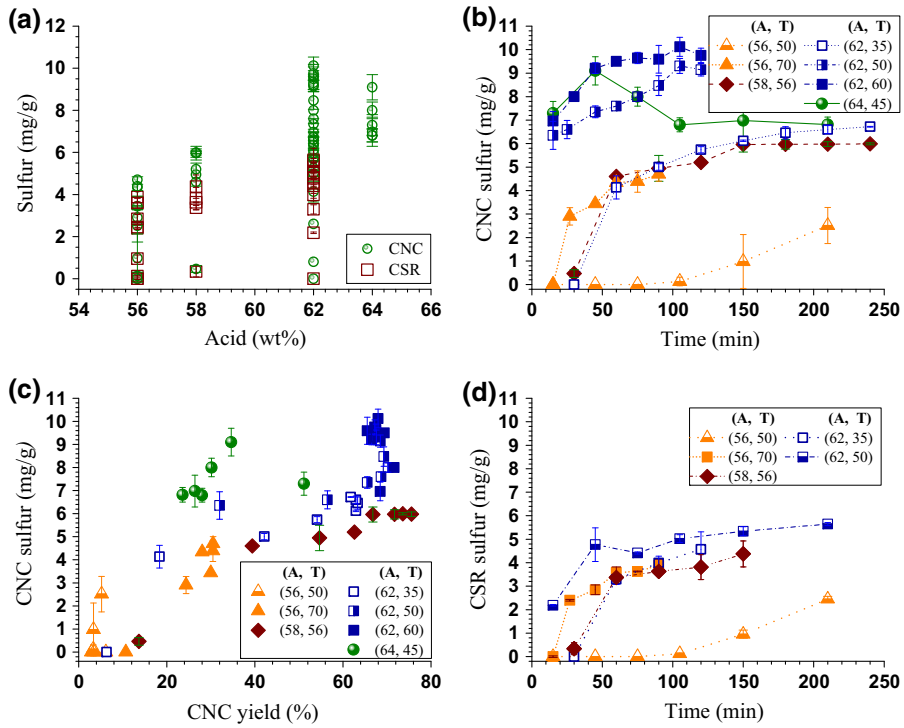

Fig. 5 Measured sulfur content. **a** Effect of acid concentration on CNC sulfur content; **b** Effect of reaction time on CNC sulfur content; **c** correlations between CNC sulfur content and CNC yield under different reaction conditions; **d** Effect of reaction time on the sulfur content of cellulose solid residue (CSR)

between CNC sulfur content and yield (except the data point at 15 min with yield 51 % in Fig. 5c).

The sulfur content of CSRs always increased with increasing reaction severity (i.e., acid concentration, temperature, reaction time) (Fig. 5d). At high reaction

severities more cellulose fibers were depolymerized to CNC and sugars and CSR no longer existed (Fig. 1), therefore, no reduction in CSR sulfur content was observed.

Conclusions

Cellulose nanocrystal (CNC) is a renewable nanomaterial that holds great promise for a variety of applications. However, literature reports of basic properties and yield of CNC were from hydrolysis conditions that produce the highest crystallinity by overly depolymerizing cellulose using a standard acid concentration of approximately 64 wt%. Consequently, low CNC yields of approximately 30 % and almost identical CNC properties were reported. Here, we demonstrated that CNC with different yields and different characteristics, such as crystal morphology or aspect ratio, crystallinity, and degree of sulfation can be obtained by slightly reducing acid concentration in the hydrolysis reactions. The results presented in this study have significant implications to a variety of practical utilizations of CNC.

Acknowledgments This work was conducted while Chen and Wang were visiting Ph.D students at the US Forest Service, Forest Products Laboratory (FPL), Madison, WI, and on official government time of Zhu, Baez, and Hirth. This work was supported by US Forest Service. Financial support included the USDA Agriculture and Food Research Initiative (AFRI) Competitive Grant (No. 2011-67009-20056), Chinese Scholarship Council (CSC), Guangzhou Elite Project of China. Funding from these programs made the visiting appointments of Chen and Wang at FPL possible. We also would like to acknowledge Drs. Ulrich Baxa of Nanotechnology Characterization Laboratory, Frederick National Laboratory for Cancer Research and Robin Harris of Johannes Gutenberg-University, Germany, for their insightful discussion on TEM images.

References

Agarwal UP, Reiner RS, Ralph SA (2010) Celulose I crystallinity determination using FT-Raman spectroscopy: univariate and multivariate methods. Cellulose 17(4):721–733

Araki J, Wada M, Kuga S, Okano T (1998) Flow properties of microcrystalline cellulose suspension prepared by acid treatment of native cellulose. Colloids Surf A 142:75–82

Beck S, Bouchard J, Berry R (2011) Controlling the reflection wavelength of iridescent solid films of nanocrystalline cellulose. Biomacromolecules 12(1):167–172

Beck-Candanedo S, Roman M, Gray DG (2005) Effect of reaction conditions on the properties and behavior of wood cellulose nanocrystal suspensions. Biomacromolecules 6:1048–1054

Biyani MV, Foster EJ, Weder C (2013) Light-healable supramolecular nanocomposites based on modified cellulose nanocrystals. ACS Macro Lett 2(3):236–240

Bondeson D, Mathew A, Oksman K (2006) Optimization of the isolation of manocrystals from microcrystalline cellulose by acid hydrolysis. Cellulose 13:171–180

Camarero Espinosa S, Kuhnt T, Foster EJ, Weder C (2013) Isolation of thermally stable cellulose nanocrystals by phosphoric acid hydrolysis. Biomacromolecules 14(4): 1223–1230

Capadona JR, Shanmuganathan K, Tyler DJ, Rowan SJ, Weder C (2008) Stimuli-responsive polymer nanocomposites inspired by the sea cucumber dermis. Science 319(5868): 1370–1374

Chen Y, Liu C, Chang PR, Cao X, Anderson DP (2009) Bionanocomposites based on pea starch and cellulose nanowhiskers hydrolyzed from pea hull fibre: effect of hydrolysis time. Carbohydr Polym 76(4):607–615

Coulibaly S, Roulin A, Balog S, Biyani MV, Foster EJ, Rowan SJ, Fiore GL, Weder C (2014) Reinforcement of optically healable supramolecular polymers with cellulose nanocrystals. Macromolecules 47(1):152–160

Davis MW (1998) A rapid modified method for compositional carbohydrate analysis of lignocellulosics by high pH anion-exchange chromatography with pulsed amperometric detection (HPAEC/PAD). J Wood Chem Technol 18(2):235–352

Dong XM, Gray DG (1997) Induced circular dichroism of isotropic and magnetically-oriented chiral nematic suspensions of cellulose crystallites. Langmuir 13(11):3029–3034

Dong XM, Revol JF, Gray DG (1998) Effect of microcrystallite preparation conditions on the formation of colloid crystals of cellulose. Cellulose 5:19–32

Habibi Y, Lucia LA, Rojas OJ (2010) Cellulose nanocrystals: chemistry, self-assembly, and applications. Chem Rev 110(6):3479–3500

Hamad WY, Hu TQ (2010) Structure–process–yield interrelations in nanocrystalline cellulose extraction. Can J Chem Eng 88:392–402

Hsu L, Weder C, Rowan SJ (2011) Stimuli-responsive, mechanically-adaptive polymer nanocomposites. J Mater Chem 21(9):2812–2822

Kargarzadeh H, Ahmad I, Abdullah I, Dufresne A, Zainudin SY, Sheltami RM (2012) Effects of hydrolysis conditions on the morphology, crystallinity, and thermal stability of cellulose nanocrystals extracted from kenaf bast fibers. Cellulose 19(3):855–866

Kelly JA, Shukaliak AM, Cheung CCY, Shopsowitz KE, Hamad WY, MacLachlan MJ (2013) Responsive photonic hydrogels based on nanocrystalline cellulose. Angew Chem Int Ed 52(34):8912–8916

Luo X, Gleisner R, Tian S, Negron J, Horn E, Pan XJ, Zhu JY (2010) Evaluation of mountain beetle infested lodgepole pine for cellulosic ethanol production by SPORL pretreatment. Ind Eng Chem Res 49(17):8258–8266

Marchessault RH, Morehead FF, Koch MJ (1961) Some hydrodynamic properties of neutral suspensions of cellulose crystallites as realted to size and shape. J Colloid Sci 16:327–344

Mukherjee SM, Woods HJ (1953) X-ray and electron microscope studies of the degradation of cellulose by sulphuric acid. Biochim Biophys Acta 10:499–511

Park S, Baker JO, Himmel ME, Parilla PA, Johnson DK (2010) Ceseealrlcuh lose crystallinity index: measurement techniques and their impact on interpreting cellulase performance. Biotechnol Biofuels 3:10

Potter KA, Jorfi M, Householder KT, Foster EJ, Weder C, Capadona JR (2014) Curcumin-releasing mechanically adaptive intracortical implants improve the proximal neuronal density and blood-brain barrier stability. Acta Biomater 10(5):2209–2222

Revol J-F, Godbout DL, Gray DG; Pulp and Paper Research Institute of Canada, assignee (1997) Solidified liquid crystals of cellulose with optically variable properties. US Patent 5, 629, 055

Revol J-F, Godbout L, Dong X-M, Gray DG, Chanzy H, Maret G (1994) Chiral nematic suspensions of cellulose crystallites; phase separation and magnetic field orientation. Liq Cryst 16:127–134

Segal L, Creely JJ, Martin AE, Conrad CM (1959) An empirical method for estimating the degree of crystallinity of native cellulose using the X-ray diffractometer. Text Res J 29:786–794

Šturcová A, Davies GR, Eichhorn SJ (2005) Elastic modulus and stress-transfer properties of tunicate cellulose whiskers. Biomacromolecules 6(2):1055–1061

Wang QQ, Zhu JY, Reiner RS, Verrill SP, Baxa U, McNeil SE (2012) Approaching zero cellulose loss in cellulose nanocrystal (CNC) production: recovery and characterization of cellulosic solid residues (CSR) and CNC. Cellulose 19(6):2033–2047

Wang Q, Zhao X, Zhu JY (2014) Kinetics of strong acid hydrolysis of a bleached kraft pulp for producing cellulose nanocrystals (CNCs). Ind Eng Chem Res 53(27):11007–11014

Xu X, Wang H, Jiang L, Wang X, Payne SA, Zhu JY, Li R (2014) Comparison between cellulose nanocrystal and cellulose nanofibril reinforced poly(ethylene oxide) nanofibers and their novel shish-kebab-like crystalline structures. Macromolecules 47(10):3409–3416

Yu H, Qin Z, Liang B, Liu N, Zhou Z, Chen L (2013) Facile extraction of thermally stable cellulose nanocrystals with a high yield of 93 % through hydrochloric acid hydrolysis under hydrothermal conditions. J Mater Chem A 1(12):3938–3944

Zhou Y, Fuentes-Hernandez C, Khan TM, Liu JC, Hsu J, Shim JW, Dindar A, Youngblood JP, Moon RJ, Kippelen B (2013) Recyclable organic solar cells on cellulose nanocrystal substrates. Sci Rep 3:1536